

V2I-Calib: A Novel Calibration Approach for Collaborative Vehicle and Infrastructure LiDAR Systems

Qianxin Qu¹, Yijin Xiong¹, Xin Wu¹, Hanyu Li¹ and Shichun Guo¹

Abstract—Cooperative vehicle and infrastructure LiDAR systems hold great potential, yet their implementation faces numerous challenges. Calibration of LiDAR systems across heterogeneous vehicle and infrastructure endpoints is a critical step to ensure the accuracy and consistency of perception system data, necessitating calibration methods that are real-time and stable. To this end, this paper introduces a novel calibration method for cooperative vehicle and road infrastructure LiDAR systems, which exploits spatial association information between detection boxes. The method centers around a novel Overall IoU metric that reflects the correlation of targets between vehicle and infrastructure, enabling real-time monitoring of calibration results. We search for common matching boxes between vehicle and infrastructure nodes by constructing an affinity matrix. Subsequently, these matching boxes undergo extrinsic parameter computation and optimization. Comparative and ablation experiments on the DAIR-V2X dataset confirm the superiority of our method. To better reflect the differences in calibration results, we have categorized the calibration tasks on the DAIR-V2X dataset based on their level of difficulty, enriching the dataset’s utility for future research. Our project is available at <https://github.com/MassimoQu/v2i-calib>.

I. INTRODUCTION

Perception systems are crucial for ensuring the safe and effective operation of autonomous vehicles [1]. Vehicle-to-infrastructure (V2I) cooperative systems can enhance the reliability of perception systems in complex traffic scenarios or adverse weather conditions by complementing vehicle-end and road-end information [2]. Collaborative vehicle and roadside LiDAR systems hold significant potential, yet their realization faces numerous challenges, especially in the calibration of sensor systems.

Calibration of LiDAR systems across heterogeneous vehicle and infrastructure endpoints is a vital step to ensure the accuracy and consistency of perception system data. This requires high-precision synchronization and registration techniques to integrate LiDAR data from both vehicles and infrastructure [3]. This not only involves complex technical issues such as time synchronization, spatial alignment, and

*This work was not supported by any organization

This work was supported by the National High Technology Research and Development Program of China under Grant No. 2018YFE0204300, and the National Natural Science Foundation of China under Grant No. U1964203, and the Guoqiang Research Institute Project No. 2019GQG1010, and the China Postdoctoral Science Foundation No. 2021M691780, and sponsored by Tsinghua University - Meituan Joint Institute for Digital Life and Tsinghua University-Didi Joint Research Center for Future Mobility.

¹ Qianxin Qu, Yijin Xiong, Xin Wu, Hanyu Li and Shichun Guo are with the State Key Laboratory of Automotive Safety and Energy, and the School of Vehicle and Mobility, Tsinghua University, Beijing, 100084, China. qqxmassimo@gmail.com; 957038131@qq.com; 2228935929@qq.com; lhy20271240@outlook.com; 370441373@qq.com

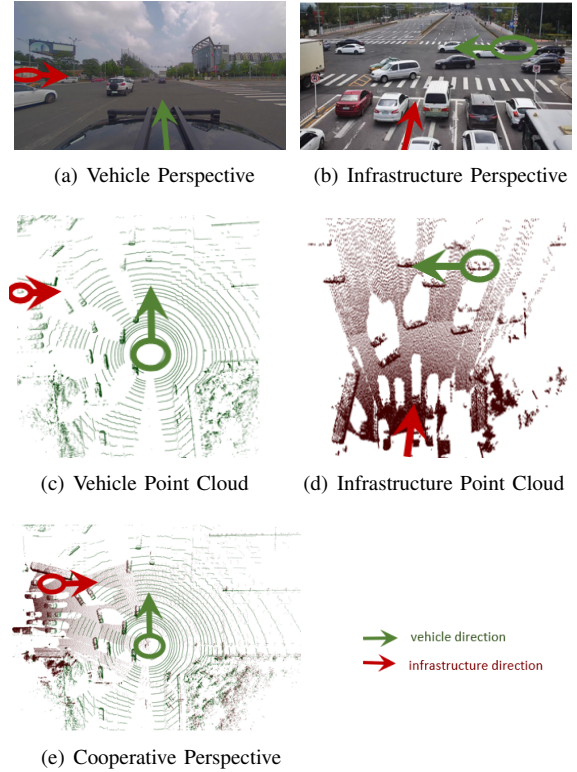


Fig. 1: Cooperative Vehicle and Infrastructure LiDAR Calibration Schematic.

data fusion but also necessitates real-time processing capabilities in dynamic environments.

To tackle these challenges, the research community has recently seen the emergence of novel approaches. These methods have successfully addressed the issue of time synchronization in collaborative vehicle and infrastructure LiDAR systems [4] [5], ensuring real-time data transmission and the accuracy of data fusion [6]. Despite advancements in spatial alignment, there remain outstanding issues such as the acquisition of spatial initial values [7], the high computational load involved in cross-source point cloud registration [8], or the substantial preliminary costs associated with point cloud mapping techniques [9]. Consequently, achieving spatial alignment in a dynamic environment for vehicle-infrastructure cooperative perception systems while maintaining low computational overhead remains a formidable challenge.

This paper presents a novel calibration method for co-

operative vehicle and infrastructure LiDAR systems. The method establishes an affinity matrix for vehicular and roadside nodes based on the Overall IoU metric, enabling the identification of shared matching boxes between vehicle and infrastructure endpoints. Subsequently, it computes and refines the extrinsic parameters associated with matched boxes. The method offers several advantages. Firstly, the proposed method does not require initial extrinsic parameters and meets real-time operation requirements. Secondly, it leverages common target information inherent to traffic scenes, enhancing its generalizability. Furthermore, compared to [10], it exclusively utilizes perception information from target detection, resulting in lower computational complexity and reduced data transmission costs, thereby offering greater potential for practical application. Lastly, V2I-Calib is designed with flexibility, having its components well decoupled, which facilitates easy adaptation to meet specific real-world requirements.

The innovations of this paper include:

- 1) We introduce the Overall IoU metric, which monitors the real-time calibration performance of extrinsic parameters. Central to this, we propose a method for constructing an affinity matrix for vehicle-road nodes, encoding the correlation between vehicular and roadside targets.
- 2) We propose a calibration method for cooperative vehicle and infrastructure LiDAR systems that thoroughly exploits the spatial associations between detection boxes, characterized by its independence from initial extrinsic parameter values and real-time capabilities.
- 3) The effectiveness of our method is validated through comparative and ablation experiments on the DAIR-V2X dataset, which is also classified according to the difficulty levels of the calibration tasks.

The contents of this paper are organized into the following sections. Initially, in Section II, we will provide a detailed review of the existing vehicle-infrastructure LiDAR calibration methods. Subsequently, in Section III, we will elaborate on the calibration method introduced in this paper, along with its constituent modules. Furthermore, in Section IV, we will conduct experiments to validate the effectiveness of our proposed method. Lastly, the paper will conclude with a summary and future outlook in Section V.

II. RELATED WORK

Point cloud registration can be categorized into same-source and cross-source registration. In essence, the calibration challenge for disparate vehicle and infrastructure LiDAR systems broadly constitutes a cross-source point cloud registration issue [11].

While significant advancements have been made in the registration tasks for same-source point clouds [12] [13] [14], cross-source point cloud registration in vehicle-infrastructure cooperative systems continues to face challenges. Compared to standard point cloud registration, the task is complicated by a combination of factors such as noise, outliers, density variation, partial overlaps, and scale

differences. However, compared to other cross-source point cloud registration tasks[8], vehicle-infrastructure cooperative systems benefit from more consistent and stable information inherent in traffic scenarios, such as elements of traffic participation including pedestrians, vehicles, and traffic signs.

Calibration methods for vehicle-infrastructure LiDAR systems can be categorized based on the source of information used during the calibration process: methods based on high-precision maps and those based on perception results.

High-precision map-based calibration methods align point cloud data collected by vehicle-mounted LiDAR with pre-constructed high-accuracy maps to achieve precise spatial calibration [9] [15]. The advantage of these methods is their utilization of rich environmental information in high-precision maps for stable and reliable calibration. However, they are limited by their reliance on high-quality map data, and the updating and maintenance of these maps pose a challenge. Therefore, these methods are most applicable in relatively stable environments, such as urban arteries and highways, where high-precision maps are available.

Perception result-based calibration methods achieve calibration by identifying and matching prominent features in the environment, such as road markings and traffic signs. These are essentially feature-based calibration methods [16][17], adapted with systematic approaches to feature extraction algorithms known as perception algorithms in the context of autonomous driving. These methods often employ multiple perception algorithms [10] to increase robustness through redundancy but may not perform well in terms of real-time processing. Some approaches combine existing perception algorithms with custom-designed feature extraction modules [18], but the general applicability of these methods across diverse scenarios requires further validation. Other methods attempt to incorporate prior information, such as location, to achieve better spatio-temporal calibration [7], yet their effectiveness at larger data scales remains to be tested.

III. METHODOLOGY

In this study, we introduce a novel vehicle-infrastructure LiDAR calibration method (V2I-Calib), the overall workflow of which is illustrated in Figure 2. The following sections will first define the problem of extrinsic parameter estimation, and then provide a detailed explanation of the proposed method and its individual components.

A. Problem Formulation

Traditional point cloud registration methods typically seek a rotation matrix \mathbf{R} and translation vector \mathbf{t} that transform one point cloud \mathbf{P}_1 onto another \mathbf{P}_2 by minimizing their discrepancy. Mathematically, this is articulated as finding the minimum of an objective function $E(\mathbf{R}, \mathbf{t})$, where E is usually a measure of distance between the point clouds:

$$\min_{\mathbf{R}, \mathbf{t}} E(\mathbf{P}_1, \mathbf{R}\mathbf{P}_2 + \mathbf{t}) \quad (1)$$

However, in the context of vehicle-infrastructure (V2I) cooperation, the point clouds from the vehicle and infrastructure inherently exhibit significant discrepancies, to which

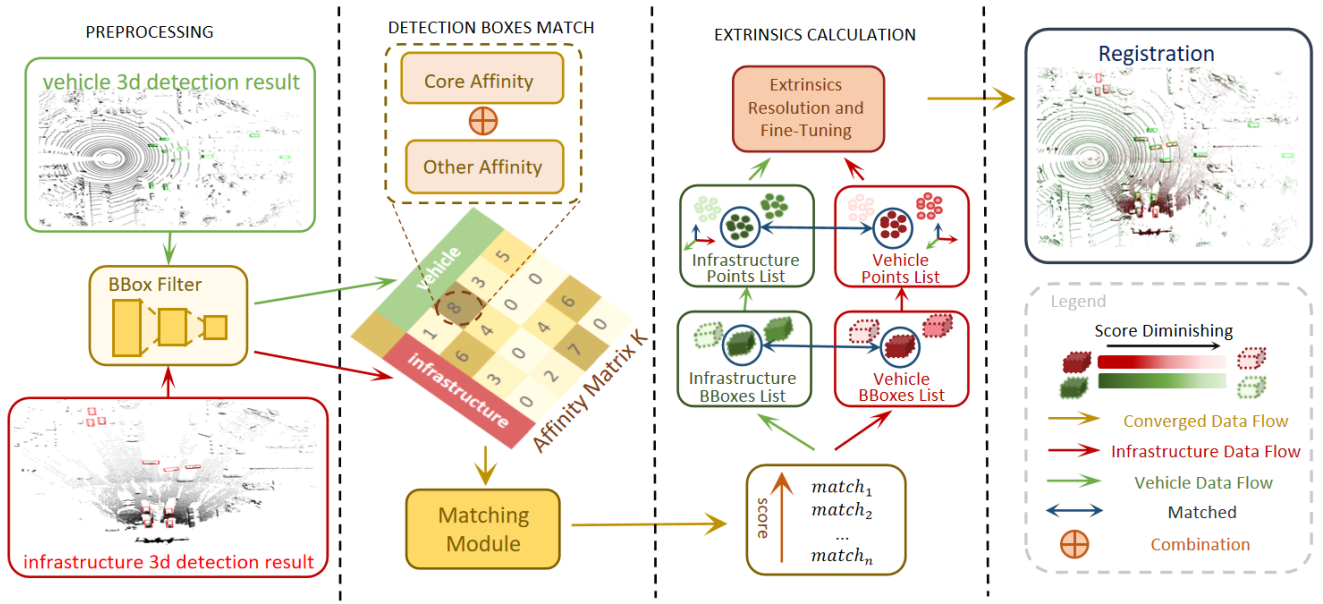


Fig. 2: V2I-Calib Workflow. The method starts with two sets of detection boxes obtained from both vehicle and infrastructure ends. We construct an affinity matrix for vehicle-road nodes using Core affinity and Other affinity. Utilizing matching algorithms, we identify common detection boxes that are matched across the vehicle and infrastructure, after which we proceed to calculate and optimize the extrinsic parameters.

the traditional methods may not be directly applicable. In response, this paper introduces a detection-box-based method. The main concept is to exploit the spatial information of detection boxes shared between the vehicle and infrastructure.

Specifically, let $\mathbf{B}^{(\text{veh})}$ denote the set of detection boxes from the vehicle, and $\mathbf{B}^{(\text{inf})}$ those from the infrastructure. Our objective is to identify the common detection box set $\mathbf{B}^{(c)}$, comprising the common targets detected by both systems. Mathematically, the common detection box set is expressed as:

$$\mathbf{B}^{(c)} = \{\mathbf{B} \mid \mathbf{B} \in \mathbf{B}^{(v)} \cap \mathbf{B}^{(i)}\} \quad (2)$$

After extracting these common detection boxes from the original point clouds, we transform them into abstract point clouds $\mathbf{P}^{(c)}$. This transformation process involves mapping the vertices of detection boxes to point sets, which we denote with the function $\text{Vertices}(\cdot)$. Thus, for each common detection box $\mathbf{B} \in \mathbf{B}^{(c)}$, its corresponding abstract point cloud is defined as:

$$\mathbf{P}^{(c)} = \bigcup_{\mathbf{B} \in \mathbf{B}^{(c)}} \text{Vertices}(\mathbf{B}) \quad (3)$$

Ultimately, the goal is to obtain the optimal extrinsic parameters \mathbf{T} by minimizing the distance between corresponding abstract point clouds:

$$\min_{\mathbf{R}, \mathbf{t}} E(\mathbf{P}_1^{(c)}, \mathbf{R}\mathbf{P}_2^{(c)} + \mathbf{t}) \quad (4)$$

$$\mathbf{T} = \begin{bmatrix} \mathbf{R} & \mathbf{t} \\ \mathbf{0}^T & 1 \end{bmatrix} \quad (5)$$

By employing this abstract point cloud registration method based on common detection boxes, we can effectively tackle the challenges of cross-source point cloud registration in V2I cooperative scenarios. The crux of the issue now becomes how to identify the common detection box set $\mathbf{B}^{(c)}$ and then fine-tune the extrinsics, which will be elaborated in subsequent chapters.

B. Affinity Formulation

In this section, we delve into the process of formulating affinity measures, a pivotal step within the vehicle-infrastructure cooperative LiDAR calibration framework. By crafting a meticulously designed affinity function, we are able to effectively evaluate the congruence between vehicle-side and infrastructure-side detection boxes, providing accurate input data for the subsequent matching module. There are two primary challenges in this process: firstly, the vehicle and infrastructure detection boxes are situated in distinct coordinate systems, complicating the direct utilization of their corresponding geometric relationships; secondly, the randomness inherent in cross-source point cloud perceptions makes distinguishing shared and single-end detection objects in real-world scenarios difficult.

Our work ingeniously addresses these issues through the introduction of a hypothesized matching pairs strategy and the oIoU metric. Below, we will describe the formulation of affinity measures in two parts: core affinity and additional affinities.

1) *Core Affinity*: The idea behind formulating the Core Affinity is to explore the scene matching scores of the available detection box pairs from both the vehicle and infrastructure. To this end, this section introduces the Overall

Intersection over Union (oIoU) as a metric to gauge the degree of scene matching. Here is the mathematical expression:

$$oIoU = \frac{1}{\max(m, n)} \sum_{i=0}^{m-1} \sum_{j=0}^{n-1} IoU_{3D}(\mathbf{BBox}_{infra,i}, \mathbf{BBox}_{vehicle,j}) \quad (6)$$

$$IoU_{3D}(\mathbf{A}, \mathbf{B}) = \frac{\text{Vol}(\mathbf{A} \cap \mathbf{B})}{\text{Vol}(\mathbf{A} \cup \mathbf{B})} \quad (7)$$

where m and n represent the number of 3d detection boxes detected by the infrastructure and the vehicle, respectively. $\mathbf{BBox}_{infra,i}$ and $\mathbf{BBox}_{vehicle,j}$ are the i -th and j -th 3d detection boxes detected by the infrastructure and the vehicle, respectively. $IoU_{3D}(\cdot)$ is the 3d intersection over union function, which calculates the volumetric overlap between 3d detection boxes. $\text{Vol}(\cdot)$ denotes the volume of a 3D detection box, and \cap and \cup represent the intersection and union in the 3D space of the detection boxes, respectively. The complexity of the naive traversal algorithm is $O(m * n)$.

The oIoU metric extends beyond the conventional IoU measure, which traditionally concentrates on the correspondence of individual box pairs. The oIoU fully leverages the positional relationships between 3D detection boxes, innovatively providing a comprehensive assessment of the spatial alignment quality within detection scenarios.

Building upon this foundation, the process of constructing Core Affinity, as illustrated in Figure 3, employs the concept of hypothetical matching pairs to define the feasible range of extrinsic parameters search between the vehicle and the infrastructure, as per the method outlined in [19]. The oIoU metric is then applied to assess the quality of spatial alignment for the corresponding extrinsic parameters of these tentative vehicle-infrastructure matching pairs.

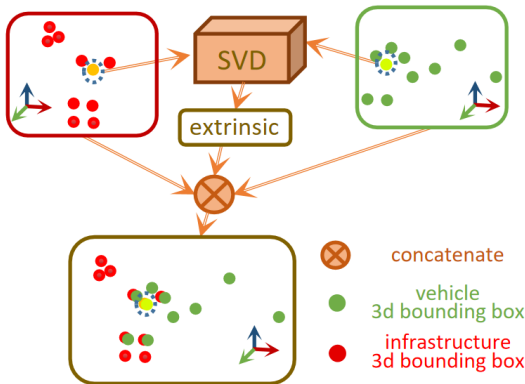


Fig. 3: Core Affinity Calculation: two 3D detection boxes are selected from the infrastructure end (red) and the vehicle end (green) as assumed matching pairs to compute the extrinsic parameters at that instance. The entire scene is then transformed and merged to calculate the scene affinity using the overlap IoU (oIoU) metric.

2) *Additional Affinity Calculation:* Beyond the core affinity, this section delves into additional affinity metrics aimed at bolstering the precision and durability of the matching

process. One such metric is category affinity, which evaluates the congruence of categories between detection boxes on the vehicle and infrastructure sides in the assumed matching pairs. This consideration is pivotal in diminishing the computational demands associated with core affinity, by ensuring that only detection boxes of matching categories are compared, thereby streamlining the matching process and enhancing its efficiency.

Furthermore, affinities such as size affinity, tracking ID affinity, angle affinity, and length affinity from VIPS[7], as well as appearance affinity from DeepSORT[20], can serve as supplements specific to scenarios to enhance the calibration stability of vehicle-infrastructure LiDAR systems in environments where shared objects are sparse.

In general scenarios, a combination of Core Affinity and Category Affinity proves to be effective, as demonstrated in section IV.

C. Affinity Matrix Formulation and Matching

The primary objective of this module involves constructing an affinity matrix based on the affinity calculation methods, with the aim of identifying the shared matching pairs among vehicle-infrastructure detection boxes.

Our method views the detection boxes as nodes, building weighted graphs G_{veh} and G_{inf} for the vehicle and infrastructure sides, respectively. At this point, the formulation of the affinity matrix and matching issue can be abstracted as a graph matching problem [21]. We can reformulate it into a quadratic assignment problem [22], described by the vertex affinity matrix K_p and the edge affinity matrix K_q . However, since the quadratic assignment problem is NP-Hard, its computational complexity can easily become a bottleneck in vehicle-infrastructure collaborative scenarios.

We simplify it by integrating the vertex affinity matrix K_p and the edge affinity matrix K_q , reducing it to a linear assignment problem. For each element $K_p(i, j)$, we consider all edges associated with node i and node j . Let $E(i)$ be the set of all edges connected to node i , and let $K_q(u, v)$ denote the affinity between edges u and v . The fusion function $F(\cdot)$ integrates the corresponding elements in K_q with $K_p(i, j)$, for all $u \in E(i)$ and $v \in E(j)$, resulting in the formation of the affinity matrix A . The problem is briefly described by the following formula:

$$A(i, j) = F(K_p(i, j), \{K_q(u, v) | u \in E(i), v \in E(j)\}) \quad (8)$$

After obtaining the affinity matrix that reflects the association degree of vehicle-infrastructure nodes, we can employ the Hungarian matching method [23] to find the optimal match within polynomial time. The transition from a quadratic to a linear matching problem might somewhat diminish the ability to independently adjust various affinities. Nonetheless, this simplification aligns well with the needs of our proposed methodology, which merges core and category affinities. Importantly, it significantly lowers the computational complexity of the matching process.

D. Extrinsic Resolution and Optimization

The aim of this section is to compute the extrinsic parameters from one or more pairs of matched detection boxes and to ensure the accuracy of these parameters. This process confronts two major challenges: first, the correspondence of the eight point pairs within the matched detection boxes is unknown, as this information is affected by the rotation matrix of the extrinsic parameters; second, the calibration of extrinsic parameters presents itself as an inherently ill-posed issue, necessitating a good initial estimate to strike a balance between accuracy and computational expense.

To address these challenges, let $\mathcal{B} = \{(\mathbf{B}_i^{(\text{inf})}, \mathbf{B}_i^{(\text{veh})})\}_{i=1}^n$ denote the set of matched detection box pairs, where $\mathbf{B}_i^{(\text{inf})}$ and $\mathbf{B}_i^{(\text{veh})}$ are the detection boxes from the infrastructure and vehicle, respectively. Based on Equation 3, we derive abstract point clouds $\mathbf{P}^{(\text{inf})}$ and $\mathbf{P}^{(\text{veh})}$, which encapsulate the vertex data from matched detection boxes. This transformation redefines the initial cross-source point cloud calibration challenge into a standardized point set registration problem.

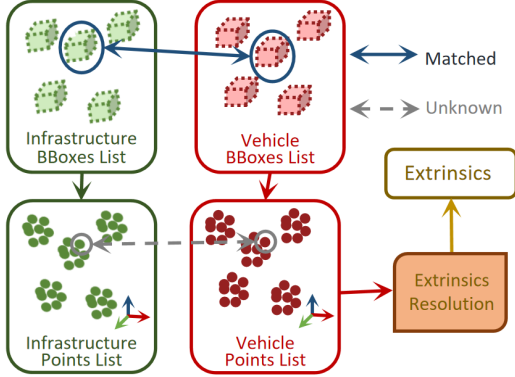


Fig. 4: Extrinsic Resolution Process. This schematic depicts the stages involved in deriving extrinsic parameters from matched detection boxes. The diagram illustrates the challenges of partial correspondence within the two points lists.

The abstract point clouds exhibit a unique partial correspondence relationship. Specifically, for each i , the group created by the bijective mapping between the vertices of $\mathbf{B}_i^{(\text{inf})}$ and $\mathbf{B}_i^{(\text{veh})}$ sets up a group-level correspondence. Nonetheless, the internal correspondence among the point pairs within \mathcal{C}_i remains unguaranteed.

$$\forall k \in \{8i, \dots, 8i + 7\}, \quad \exists \mathbf{p}_k^{(\text{inf})} \leftrightarrow \mathbf{p}_k^{(\text{veh})} \quad (9)$$

where $\mathbf{p}_k^{(\text{inf})}$ and $\mathbf{p}_k^{(\text{veh})}$ are the points in $\mathbf{P}^{(\text{inf})}$ and $\mathbf{P}^{(\text{veh})}$ respectively, originating from the vertices of the i -th matched detection box pair in the dataset.

Based on this characteristic, applying a naive point cloud extrinsic parameter calculation method [19] can provide an rough initial value of the extrinsics. Subsequently, based on this initial value, extrinsic parameter optimization is conducted [24][25] to derive the optimal extrinsic parameter values.

IV. EXPERIMENT

In this chapter, we will provide a detailed overview of the experimental design, evaluation metrics, dataset characteristics, and specific experimental settings for assessing the performance of our proposed V2I-Calib method.

A. Evaluation Metrics

The core metrics for experimental evaluation include Relative Rotation Error (RRE), Relative Translation Error (RTE), and Success Rate.

Relative Rotation Error (RRE): Measures the accuracy of the rotation component in the calibration result, i.e., the angular difference between the estimated rotation matrix \mathbf{R}_e and the ground truth \mathbf{R}_t .

$$\theta_{\text{degrees}} = \arccos\left(\frac{\text{tr}(\Delta\mathbf{R}) - 1}{2}\right) \times \frac{180}{\pi} \quad (10)$$

$$\Delta\mathbf{R} = \mathbf{R}_t^{-1}\mathbf{R}_e \quad (11)$$

Relative Translation Error (RTE): Evaluates the accuracy of the translation vector in the calibration result, i.e., the distance difference between the estimated translation vector \mathbf{t}_e and the ground truth translation vector \mathbf{t}_t .

$$RTE = \|\mathbf{t}_t^{-1} - \mathbf{t}_e\|_2 \quad (12)$$

Success Rate: Defined as the proportion of successfully completed calibration tasks within a preset error threshold, reflecting the method's robustness and reliability. Following the criteria in [7], we consider $RTE < 2m$ as the determinant criterion.

These metrics can provide information on the adaptability and stability of the method across different scenarios.

B. Datasets

In this study, we conducted experimental validation using the DAIR-V2X dataset[26], which encompasses a wealth of data collected from Vehicle-Infrastructure Cooperative Autonomous Driving (VICAD) scenarios, including vehicular and infrastructural LiDAR data along with their 3D box annotations. The specifications of the vehicular and roadside LiDAR systems are presented in Table I.

TABLE I: Specifications of LiDAR Equipment

Parameter	Roadside LiDAR	Vehicle LiDAR
LiDAR Points	300 lines	40 lines
Horizontal Field of View	100°	360°
Max Detection Range	280 meters	200 meters

To enhance the assessment of our method's effectiveness across varied scenarios, we have instituted a data difficulty categorization. While conventional perception datasets like KITTI have established a difficulty rating based on factors such as the count, dimensions, and levels of occlusion or truncation of objects, similar frameworks for calibration tasks within publicly available datasets are notably absent.

Mindful of scenario classifications in extant literature and the absence of established difficulty metrics for calibration, we have methodically classified the DAIR-V2X dataset into distinct levels of difficulty, making the criteria and associated experimental code readily accessible.

Our approach to defining data difficulty draws from the established logic used in perception tasks, factoring in the intricacy of the environment, the spatial relation between vehicles and infrastructure, and the presence of shared objects within the scene. For instance, we utilized categories from the KITTI dataset[27]—such as object count, size, and states of occlusion or truncation—as a basis to evaluate their influence on the calibration process for LiDAR systems between vehicles and infrastructure. It’s important to note that we also accounted for the effect of relative positioning within vehicular-roadside scenarios and the possibility of missing shared objects in counter scenarios, highlighting that a shared zone in point clouds can enable the gathering of required shared objects by broadening the detection range, albeit potentially at the expense of increased detection time.

C. Experimental Settings

In this section, a systematic performance evaluation of the proposed method will be conducted through comparative experiments and ablation studies. Contrast experiments are aimed at verifying the superiority of the proposed method by comparing its performance with other methods on datasets of varying difficulty. On the other hand, ablation studies further analyze the effectiveness of individual components/modules. Both experiments were conducted on an experimental platform equipped with an Intel i7-9750H CPU.

1) *Contrast Experiment*: The comparative experiments assessed the performance of the method presented in this article against other existing methods on metrics such as Rotation Error (RRE), Translation Error (RTE), and success rate. The existing methods are primarily categorized into traditional approaches represented by VGICP [12] and NDT[25], and perception-based approaches exemplified by VIPS [7] and HPCR-VI [10].

TABLE II: Comparative Results of Different Methods.

Dataset Difficulty	Methods	RRE(°)	RTE(m)	Success Rate(%)	Time (s)
easy group	VGICP [12]	3.18	6.43	6.0	0.77
	NDT [25]	1.88	6.36	6.4	19.82
	HPCR-VI [10]	5.15	0.91	81.1	/
	VIPS [7]	0.96	0.84	79.3	0.33
	V2I-Calib	0.68	0.56	96.8	0.21
hard group	VGICP [12]	3.11	6.91	4.1	0.42
	NDT [25]	2.33	3.91	6.0	29.62
	HPCR-VI [10]	6.43	1.52	43.3	/
	VIPS [7]	2.12	2.05	57.5	0.29
	V2I-Calib	1.92	1.67	71.8	0.15

As indicated in Table II, it is apparent that traditional point cloud registration algorithms largely fail on the DAIR-V2X dataset, and the existing perception-based methods exhibit

significant errors. In contrast, the method proposed in this article achieves better results in terms of both precision and real-time performance. Additionally, by incorporating detection box confidence in the engineering implementation, our method effectively mitigates the problem of calibration precision degradation under multi-target interference compared to [10]. In terms of immediacy, it meets the calibration time requirement of less than 0.35 seconds for common intersection traffic scenarios as analyzed in [18]. Notably, the running times for the methods in the more challenging group are generally lower than those in the simpler group, which is attributable to the fewer shared targets in complex scenes, reducing the computational load.

This series of experimental validations confirms that the proposed vehicle-to-infrastructure calibration method not only provides highly accurate calibration results across various scenarios but also demonstrates its feasibility in terms of immediacy, offering robust support for the practical application of vehicle-to-infrastructure LiDAR systems.

2) *Ablation experiment*: In this section, we aim to validate the effectiveness of the core affinity formulation module presented in Section III-B and the extrinsic parameter optimization module discussed in Section III-D through a series of ablation studies.

TABLE III: Methods Composition Of Different Strategies.

Method	Affinity Construction	Extrinsic Optimization
V2I-Calib-v3	Length and Angle [7]	Yes
V2I-Calib-v2	Core and Category	No
V2I-Calib-v1	Core and Category	Yes

TABLE IV: Ablation Study On Methods With Different Strategies

Dataset Difficulty	Methods	RRE(°)	RTE(m)	Success Rate(%)	Time (s)
easy group	V2I-Calib-v3	0.95	0.79	80.3	0.32
	V2I-Calib-v2	0.98	0.62	50.0	0.18
	V2I-Calib-v1	0.68	0.56	96.8	0.21
hard group	V2I-Calib-v3	2.69	2.37	57.2	0.28
	V2I-Calib-v2	1.93	1.82	53.4	0.14
	V2I-Calib-v1	1.92	1.67	71.8	0.15

Comparing V2I-Calib-v1 with V2I-Calib-v3, we observe that the core affinity formulation module proposed in this paper exhibits enhanced robustness, achieving an approximate 20% increase in the success rate compare. Moreover, we evaluated the impact of the extrinsic parameter optimization module on calibration outcomes. A comparative analysis between V2I-Calib-v1 and V2I-Calib-v2, before and after the introduction of the extrinsic optimization module, reveals that the optimization algorithm significantly improves the precision and success rate of the calibration.

To validate the superiority of the affinity metrics proposed in this paper, we conducted comparative analyses with category affinity, angle affinity, and length affinity as delineated

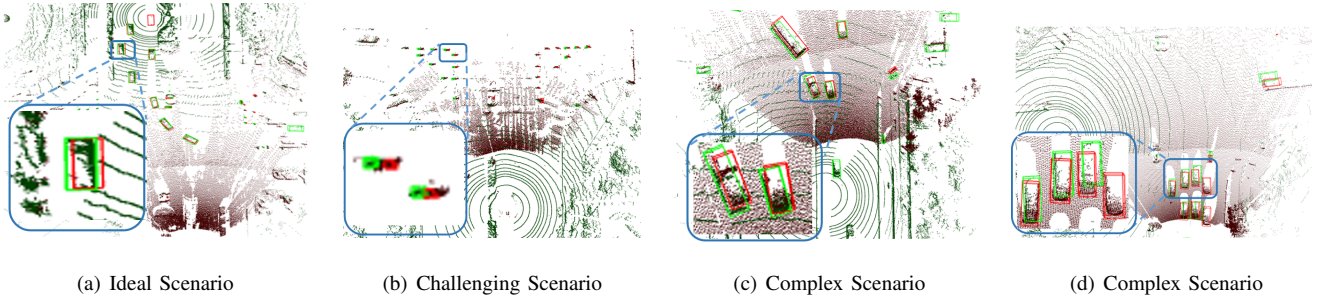


Fig. 5: Comparative Calibration Results Across Diverse Scenarios: (a) Accurate alignment of vehicle and infrastructure detection boxes. (b) Calibration errors due to small-sized detection boxes. (c, d) Good and Suboptimal calibration results combining multiple detection boxes, respectively.

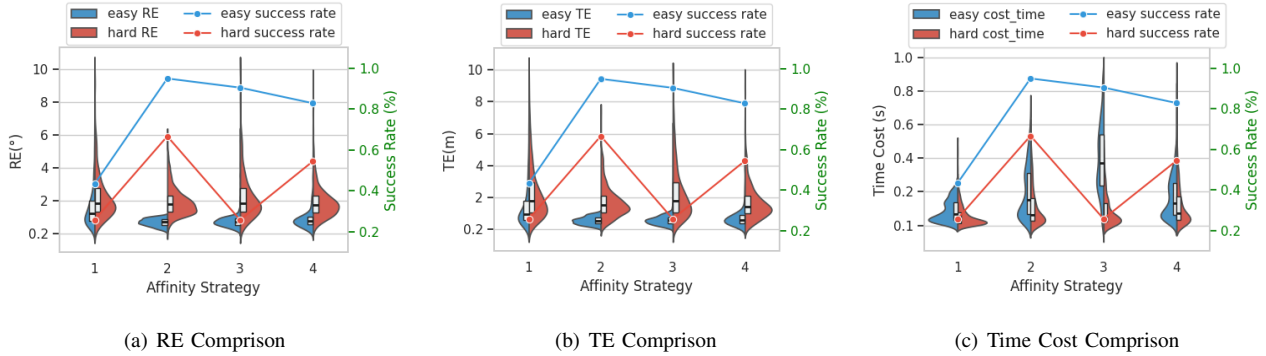


Fig. 6: Ablation Comparison of Different Affinity Strategies. The violin plots correspond to the left-side metrics of TE, RE, and Time Cost, while the line charts relate to the success rate metric on the right. We compared four strategies for constructing the affinity matrix based on different combinations of affinities: Strategy 1 combines angle affinity with category affinity, Strategy 2 combines core affinity with category affinity, Strategy 3 employs core affinity alone, and Strategy 4 combines length affinity with category affinity. It is evident that Strategy 2, utilized by our method, surpasses the other strategies in terms of both extrinsic parameter accuracy and computational time.

in [7]. The results, as depicted in Figure 6, demonstrate that Strategy 2, which is core affinity, achieves a higher success rate and extrinsic parameter accuracy within an acceptable time frame. Notably, when comparing Strategy 2 (core affinity with category affinity) with Strategy 3 (core affinity without category affinity), it is apparent that the inclusion of category affinity significantly reduces the overall computational time and notably enhances performance within the hard group.

Regarding the Strategy 1 angle affinity and Strategy 4 length affinity extended from [7], these strategies were originally designed for scenarios assisted by positional information. However, experimental results show that they are somewhat applicable in scenarios without initial extrinsic parameter values, although their performance significantly decreases in challenging settings. Upon further analysis of the scenarios where these strategies failed, we observed that most of these scenarios involved extrinsic parameters with relatively large absolute values, aligning with the limitations inherent in their initial design rationale.

These ablation studies not only confirm the efficacy of each distinct module within our framework but also under-

score their collective role in enhancing the overall functionality of the system.

V. CONCLUSIONS

This study introduces a novel calibration method, V2I-Calib, for cooperative vehicle and infrastructure LiDAR systems. Through a series of experiments, our method demonstrates superior calibration accuracy and robustness across datasets of various difficulties, particularly excelling in handling complex scenes while maintaining real-time performance. In essence, the calibration task for cooperative vehicle-infrastructure LiDAR systems is fundamentally a data association task, bearing some similarity to multi-object tracking tasks.

Future research will integrate the concept of temporal association from multi-object detection, merging spatial alignment and temporal synchronization tasks. Furthermore, the integration of 2D bounding box information will shift the research focus towards multi-sensor fusion calibration in cooperative vehicle-infrastructure systems.

As cooperative vehicle-infrastructure technology continues to evolve, we anticipate this framework to adapt to more

application scenarios, providing a solid foundation for the safety and reliability of autonomous driving systems.

REFERENCES

- [1] C. Brewitt, M. Tamborski, C. Wang, and S. V. Albrecht, "Verifiable goal recognition for autonomous driving with occlusions," in *2023 IEEE/RSJ International Conference on Intelligent Robots and Systems (IROS)*. IEEE, 2023, pp. 11 210–11 217.
- [2] J. Wang, Z. Wu, Y. Liang, J. Tang, and H. Chen, "Perception methods for adverse weather based on vehicle infrastructure cooperation system: A review," *Sensors*, vol. 24, no. 2, p. 374, 2024.
- [3] B. Cao, C.-N. Ritter, K. Alomari, and D. Goehring, "Cooperative lidar localization and mapping for v2x connected autonomous vehicles," in *2023 IEEE/RSJ International Conference on Intelligent Robots and Systems (IROS)*. IEEE, 2023, pp. 11 019–11 026.
- [4] K. Yang, D. Yang, J. Zhang, M. Li, Y. Liu, J. Liu, H. Wang, P. Sun, and L. Song, "Spatio-temporal domain awareness for multi-agent collaborative perception," in *Proceedings of the IEEE/CVF International Conference on Computer Vision*, 2023, pp. 23 383–23 392.
- [5] Z. Lei, S. Ren, Y. Hu, W. Zhang, and S. Chen, "Latency-aware collaborative perception," in *European Conference on Computer Vision*. Springer, 2022, pp. 316–332.
- [6] H. Yu, Y. Tang, E. Xie, J. Mao, P. Luo, and Z. Nie, "Flow-based feature fusion for vehicle-infrastructure cooperative 3d object detection," *Advances in Neural Information Processing Systems*, vol. 36, 2024.
- [7] S. Shi, J. Cui, Z. Jiang, Z. Yan, G. Xing, J. Niu, and Z. Ouyang, "Vips: Real-time perception fusion for infrastructure-assisted autonomous driving," in *Proceedings of the 28th Annual International Conference on Mobile Computing And Networking*, 2022, pp. 133–146.
- [8] X. Huang, G. Mei, and J. Zhang, "Cross-source point cloud registration: Challenges, progress and prospects," *Neurocomputing*, p. 126383, 2023.
- [9] K. Maruta, M. Takizawa, R. Fukatsu, Y. Wang, Z. Li, and K. Sakaguchi, "Blind-spot visualization via ar glasses using millimeter-wave v2x for safe driving," in *2021 IEEE 94th Vehicular Technology Conference (VTC2021-Fall)*. IEEE, 2021, pp. 1–5.
- [10] Y. Zhao, X. Zhang, S. Zhang, S. Qiu, H. Yin, and X. Zhang, "Hpcr-vi: Heterogeneous point cloud registration for vehicle-infrastructure collaboration," in *2023 IEEE Intelligent Vehicles Symposium (IV)*. IEEE, 2023, pp. 1–6.
- [11] X. Huang, G. Mei, J. Zhang, and R. Abbas, "A comprehensive survey on point cloud registration," *arXiv preprint arXiv:2103.02690*, 2021.
- [12] K. Koide, M. Yokozuka, S. Oishi, and A. Banno, "Voxelized gcp for fast and accurate 3d point cloud registration," in *2021 IEEE International Conference on Robotics and Automation (ICRA)*. IEEE, 2021, pp. 11 054–11 059.
- [13] A. Hertz, R. Hanocka, R. Giryes, and D. Cohen-Or, "Pointgmm: A neural gmm network for point clouds," in *Proceedings of the IEEE/CVF Conference on Computer Vision and Pattern Recognition*, 2020, pp. 12 054–12 063.
- [14] Y. Aoki, H. Goforth, R. A. Srivatsan, and S. Lucey, "Pointnetlk: Robust & efficient point cloud registration using pointnet," in *Proceedings of the IEEE/CVF conference on computer vision and pattern recognition*, 2019, pp. 7163–7172.
- [15] X. Duan, H. Jiang, D. Tian, T. Zou, J. Zhou, and Y. Cao, "V2i based environment perception for autonomous vehicles at intersections," *China Communications*, vol. 18, no. 7, pp. 1–12, 2021.
- [16] J. Jiao, Q. Liao, Y. Zhu, T. Liu, Y. Yu, R. Fan, L. Wang, and M. Liu, "A novel dual-lidar calibration algorithm using planar surfaces," in *2019 IEEE Intelligent Vehicles Symposium (IV)*. IEEE, 2019, pp. 1499–1504.
- [17] Z. Qiao, Z. Yu, H. Yin, and S. Shen, "Pyramid semantic graph-based global point cloud registration with low overlap," in *2023 IEEE/RSJ International Conference on Intelligent Robots and Systems (IROS)*. IEEE, 2023, pp. 11 202–11 209.
- [18] Y. He, L. Ma, Z. Jiang, Y. Tang, and G. Xing, "Vi-eye: semantic-based 3d point cloud registration for infrastructure-assisted autonomous driving," in *Proceedings of the 27th Annual International Conference on Mobile Computing and Networking*, 2021, pp. 573–586.
- [19] K. S. Arun, T. S. Huang, and S. D. Blostein, "Least-squares fitting of two 3-d point sets," *IEEE Transactions on pattern analysis and machine intelligence*, no. 5, pp. 698–700, 1987.
- [20] N. Wojke, A. Bewley, and D. Paulus, "Simple online and realtime tracking with a deep association metric," in *2017 IEEE international conference on image processing (ICIP)*. IEEE, 2017, pp. 3645–3649.
- [21] H. Sun, W. Zhou, and M. Fei, "A survey on graph matching in computer vision," in *2020 13th International Congress on Image and Signal Processing, BioMedical Engineering and Informatics (CISP-BMEI)*. IEEE, 2020, pp. 225–230.
- [22] F. Zhou and F. De la Torre, "Factorized graph matching," *IEEE transactions on pattern analysis and machine intelligence*, vol. 38, no. 9, pp. 1774–1789, 2015.
- [23] H. W. Kuhn, "The hungarian method for the assignment problem," *Naval research logistics quarterly*, vol. 2, no. 1-2, pp. 83–97, 1955.
- [24] P. J. Besl and N. D. McKay, "Method for registration of 3-d shapes," in *Sensor fusion IV: control paradigms and data structures*, vol. 1611. Spie, 1992, pp. 586–606.
- [25] P. Biber and W. Straßer, "The normal distributions transform: A new approach to laser scan matching," in *Proceedings 2003 IEEE/RSJ International Conference on Intelligent Robots and Systems (IROS 2003)(Cat. No. 03CH37453)*, vol. 3. IEEE, 2003, pp. 2743–2748.
- [26] H. Yu, W. Yang, H. Ruan, Z. Yang, Y. Tang, X. Gao, X. Hao, Y. Shi, Y. Pan, N. Sun, *et al.*, "V2x-seq: A large-scale sequential dataset for vehicle-infrastructure cooperative perception and forecasting," in *Proceedings of the IEEE/CVF Conference on Computer Vision and Pattern Recognition*, 2023, pp. 5486–5495.
- [27] A. Geiger, P. Lenz, and R. Urtasun, "Are we ready for autonomous driving? the kitti vision benchmark suite," in *2012 IEEE conference on computer vision and pattern recognition*. IEEE, 2012, pp. 3354–3361.